Convex Optimization Based MIMO Array Synthesis for Millimeter-Wave Imaging

Shuoguang Wang(1), Shiyong Li*(1), Ahmad Hoorfar(2), Guoqiang Zhao(1), and Houjun Sun(1)
(1) Beijing Institute of Technology, Beijing, China; e-mail: 1120131426@bit.edu.cn; lisy_98@bit.edu.cn; zhaogq1976@bit.edu.cn; sunhoujun@bit.edu.cn
(2) Villanova University,Villanova, USA; e-mail: ahmad.hoorfar@villanova.edu

Abstract

This paper proposes a convex optimization model for the multiple-input multiple-output (MIMO) array synthesis. We generate a block shaped reference pattern that occupies the entire imaging area of interest in order to involve the effect of each pixel into the optimization model. Through introducing coefficients with respect to the array elements, we can transform the array synthesis into minimization of the coefficients. Numerical results demonstrate the efficacy of the proposed method.

1 Introduction

The state-of-the-art two dimensional (2-D) antenna array-based systems can acheive real time high-resolution imaging, however, with high system cost although employing multiple-input multiple-output (MIMO) arrays to reduce the number of antenna elements [1–4]. To reap the benefits of sparseness, the number of antennas of MIMO can be further reduced by using the sparse array synthesis (SAS) method, without causing high-level grating lobes and sidelobes.

Significant efforts have been made in MIMO SAS for near-field imaging. In [5, 6], the sparse MIMO arrays were designed to have the specific topologies, such as the curvilinear and spiral arrays. The heuristic algorithms, such as the simulated annealing (SA) algorithm [7] and the swarm optimization (PSO) method [8], were also employed for the array synthesis. The work in [9, 10] employed the multi-objective covariance matrix evolution strategy (CMA-ES) algorithm to optimally design a MIMO array topology for through-the-wall radar imaging and ground-penetrating imaging.

In this paper, we propose a convex optimization method for SAS. We first introduce a sampling matrix into the data model for the purpose of selecting antennas. In so doing, the SAS problem is transformed into reconstruction of the sampling matrix, which then can be relaxed into solving a convex optimization. In order to improve the robustness of SAS, we set the reference pattern as the imaging result of the continuous scattering targets filling over the whole imaging region of interest.

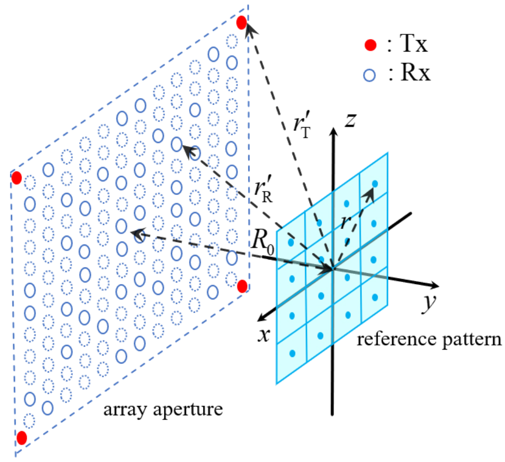

Figure 1. MIMO sparse planar array for wideband near-field imaging, where the reference pattern is set to cover all the imaging area at a fixed distance.

In addition, the proposed SAS method has the flexibility of being implemented in optimization of the transmit subarray and the receive subarray separately.

2 Formulation

We first consider a wideband MIMO sparse array as shown in Figure 1, with N_{T} transmit antennas being fixed (on its four corners in the demo topology), and the receive antennas being arbitrarily positioned. The N receive elements are sampled from the 2-D dense array. Under the Born approximation, the scattered field from the target with Q scatterers can be expressed as,

$$s(k,\boldsymbol{r}'_{\mathrm{T}},\boldsymbol{r}'_{\mathrm{R}})=\sum_{q=1}^{Q}\sigma_q\frac{e^{-\mathrm{j}k\left(\left|\boldsymbol{r}'_{\mathrm{T}}-\boldsymbol{r}_q\right|+\left|\boldsymbol{r}'_{\mathrm{R}}-\boldsymbol{r}_q\right|\right)}}{16\pi^2\left|\boldsymbol{r}'_{\mathrm{T}}-\boldsymbol{r}_q\right|\cdot\left|\boldsymbol{r}'_{\mathrm{R}}-\boldsymbol{r}_q\right|},\tag{1}$$

where $k=\frac{2\pi f}{c}$ denotes the wavenumber, and $\boldsymbol{r}'_{\mathrm{T}}$ and $\boldsymbol{r}'_{\mathrm{R}}$ represent the positions of transmit and receive elements, respectively. $\boldsymbol{r}_q$ stands for the position of the qth scatterer with the scattering coefficient of σ_q. Equation (1) can be expressed by a series of vectors with respect to k and $\boldsymbol{r}'_{\mathrm{T}}$ as follows,

$$\boldsymbol{s}(k,\boldsymbol{r}'_{\mathrm{T}})=\boldsymbol{A}_{\mathrm{R}_k}\boldsymbol{A}_{\mathrm{T}_k}\boldsymbol{\sigma},\tag{2}$$

where

$$\boldsymbol{A}_{\mathrm{R}_k}=\begin{bmatrix} \frac{e^{-\mathrm{j}k\left|\boldsymbol{r}'_{\mathrm{R}_1}-\boldsymbol{r}_1\right|}}{4\pi\left|\boldsymbol{r}'_{\mathrm{R}_1}-\boldsymbol{r}_1\right|} & \cdots & \frac{e^{-\mathrm{j}k\left|\boldsymbol{r}'_{\mathrm{R}_1}-\boldsymbol{r}_Q\right|}}{4\pi\left|\boldsymbol{r}'_{\mathrm{R}_1}-\boldsymbol{r}_Q\right|} \\ \vdots & \ddots & \vdots \\ \frac{e^{-\mathrm{j}k\left|\boldsymbol{r}'_{\mathrm{R}_N}-\boldsymbol{r}_1\right|}}{4\pi\left|\boldsymbol{r}'_{\mathrm{R}_N}-\boldsymbol{r}_1\right|} & \cdots & \frac{e^{-\mathrm{j}k\left|\boldsymbol{r}'_{\mathrm{R}_N}-\boldsymbol{r}_Q\right|}}{4\pi\left|\boldsymbol{r}'_{\mathrm{R}_N}-\boldsymbol{r}_Q\right|} \end{bmatrix}_{N\times Q} \tag{3}$$

$$\boldsymbol{A}_{\mathrm{T}_k}=\begin{bmatrix} \frac{e^{-\mathrm{j}k\left|\boldsymbol{r}'_{\mathrm{T}}-\boldsymbol{r}_1\right|}}{4\pi\left|\boldsymbol{r}'_{\mathrm{T}}-\boldsymbol{r}_1\right|} & & & \\ & \frac{e^{-\mathrm{j}k\left|\boldsymbol{r}'_{\mathrm{T}}-\boldsymbol{r}_2\right|}}{4\pi\left|\boldsymbol{r}'_{\mathrm{T}}-\boldsymbol{r}_2\right|} & & \\ & & \ddots & \\ & & & \frac{e^{-\mathrm{j}k\left|\boldsymbol{r}'_{\mathrm{T}}-\boldsymbol{r}_Q\right|}}{4\pi\left|\boldsymbol{r}'_{\mathrm{T}}-\boldsymbol{r}_Q\right|} \end{bmatrix}, \tag{4}$$

$$\boldsymbol{\sigma}=\left[\sigma_1,\sigma_2,\ldots,\sigma_Q\right]^T. \tag{5}$$

To obtain an optimization model for the synthesis of the antenna array, we introduce here a coefficient for each receive antenna, which constructs a sampling matrix $\boldsymbol{\Psi}$. Then, the echo model can be expressed by,

$$\boldsymbol{s}'(k,\boldsymbol{r}'_{\mathrm{T}})=\boldsymbol{\Psi}\boldsymbol{s}(k,\boldsymbol{r}'_{\mathrm{T}}), \tag{6}$$

where $\boldsymbol{\Psi}$ is a diagonal matrix with the diagonal elements varing from w_1 to w_N representing the coefficient with respect to each receive channel.

Using the delay-and-sum method [11], the intermediate imaging result with respect to k and $\boldsymbol{r}'_{\mathrm{T}}$ can be expressed as,

$$\boldsymbol{g}(k,\boldsymbol{r}'_{\mathrm{T}})=\boldsymbol{\Phi}_{\mathrm{T}_k}\boldsymbol{\Phi}_{\mathrm{R}_k}\boldsymbol{s}'(k,\boldsymbol{r}'_{\mathrm{T}}), \tag{7}$$

where

$$\boldsymbol{\Phi}_{\mathrm{T}_k}=4\pi\begin{bmatrix} |\boldsymbol{r}''_1-\boldsymbol{r}'_{\mathrm{T}}|e^{\mathrm{j}k|\boldsymbol{r}''_1-\boldsymbol{r}'_{\mathrm{T}}|} & & \\ & \ddots & \\ & & |\boldsymbol{r}''_M-\boldsymbol{r}'_{\mathrm{T}}|e^{\mathrm{j}k|\boldsymbol{r}''_M-\boldsymbol{r}'_{\mathrm{T}}|} \end{bmatrix} \tag{8}$$

$$\boldsymbol{\Phi}_{\mathrm{R}_k}=4\pi\begin{bmatrix} \left|\boldsymbol{r}''_1-\boldsymbol{r}'_{\mathrm{R}_1}\right|e^{\mathrm{j}k\left|\boldsymbol{r}''_1-\boldsymbol{r}'_{\mathrm{R}_1}\right|} & \cdots & \left|\boldsymbol{r}''_1-\boldsymbol{r}'_{\mathrm{R}_N}\right|e^{\mathrm{j}k\left|\boldsymbol{r}''_1-\boldsymbol{r}'_{\mathrm{R}_N}\right|} \\ \vdots & \ddots & \vdots \\ \left|\boldsymbol{r}''_M-\boldsymbol{r}'_{\mathrm{R}_1}\right|e^{\mathrm{j}k\left|\boldsymbol{r}''_M-\boldsymbol{r}'_{\mathrm{R}_1}\right|} & \cdots & \left|\boldsymbol{r}''_M-\boldsymbol{r}'_{\mathrm{R}_N}\right|e^{\mathrm{j}k\left|\boldsymbol{r}''_M-\boldsymbol{r}'_{\mathrm{R}_N}\right|} \end{bmatrix} \tag{9}$$

and $\boldsymbol{r}''_m$ represents the position of the mth imaging pixel with $m\in\{1,2,\cdots,M\}$.

Through coherent summation of the results in (7) with respect to all the possible k and $\boldsymbol{r}'_{\mathrm{T}}$, we obtain the final imaging result, such as,

$$\boldsymbol{g}=\boldsymbol{B}\boldsymbol{w}, \tag{10}$$

where

$$\boldsymbol{B}=\sum_k\sum_{\boldsymbol{r}'_{\mathrm{T}}}\boldsymbol{\Phi}_{\mathrm{T}_k}\boldsymbol{\Phi}_{\mathrm{R}_k}\boldsymbol{S}_k, \tag{11}$$

and $\boldsymbol{S}_k$ is a diagonal matrix with the diagonal elements being $s\left(k,\boldsymbol{r}'_{\mathrm{T}},\boldsymbol{r}'_{\mathrm{R}_1}\right)$ to $s\left(k,\boldsymbol{r}'_{\mathrm{T}},\boldsymbol{r}'_{\mathrm{R}_N}\right)$, and $\boldsymbol{w}=\left[w_1,w_2,\ldots,w_N\right]^T$.

As such, the SAS for the wideband near-field imaging problem can then be expressed as:

$$\boldsymbol{w}=\arg\left(\min_{\boldsymbol{w}}\|\boldsymbol{w}\|_0\right)\quad \text{s.t. } \|\boldsymbol{g}_{\mathrm{ref}}-\boldsymbol{B}\boldsymbol{w}\|_2^2\le\varepsilon, \tag{12}$$

where $\boldsymbol{w}$ is the nonzero entry of excitation values, $\boldsymbol{g}_{\mathrm{ref}}$ denotes the reference pattern, and ε is the tolerance to narrow the gap between the imaging result and the desired reference pattern. The reference pattern in this work is arranged as the continuous point targets covering the interested imaging region.

Usually, the above minimization will be relaxed into an l_1-norm based minimization [12, 14]. Here, we utilize the iterative weighted l_1-norm minimization approach [14], which can be expressed as,

$$\begin{aligned} &\boldsymbol{w}^{(i)}=\arg\left(\min_{\boldsymbol{w}}\|\boldsymbol{C}^{(i)}\boldsymbol{w}^{(i)}\|_1\right)\\ &\text{s.t. } \|\boldsymbol{g}_{\mathrm{ref}}-\boldsymbol{B}\boldsymbol{w}^{(i)}\|_2^2\le\varepsilon\\ &i=1,2,\ldots,I_{\mathrm{iter}}, \end{aligned} \tag{13}$$

where $\boldsymbol{w}^{(i)}$ is the element weight vector in the ith iteration, I_{iter} denotes the number of iterations, and $\boldsymbol{C}^{(i)}$ is a diagonal matrix with $\boldsymbol{C}^{(1)}=\boldsymbol{I}$ being an identity matrix. For $i>1$, we have the diagonal elements of $\boldsymbol{C}^{(i)}$ varing from $\frac{1}{w_1^{(i-1)}+\mu}$ to $\frac{1}{w_N^{(i-1)}+\mu}$, where μ is a constant greater than 0, which is utilized to avoid the singularity issue in $\boldsymbol{C}^{(i)}$ when $\boldsymbol{w}^{(i)}$ has a very small value. In this paper, we set μ as 0.1 in all the SAS processes.

Here, we employ the MATLAB-based CVX toolbox [15] to solve (13). Then, the desired receive array layout with the corresponding sparse weights is obtained. If both the positions of transmit and receive antennas need to be synthesized, we can fix the transmit positions and optimize the receive positions, or vice versa.

3 Numerical Results

In this section, we compare the imaging results of the arrays generated by the proposed method and those of the arrays synthesized by the state-of-the-art methods.

Here we have synthesized the sparse array with more than 100 receivers, as shown in Figure 2(a). The curvilinear array [5], the spiral array [6], and the equally spaced sparse MIMO array are provided for comparison, whose topologies are illustrated in Figures 2(b) to (d), respectively.

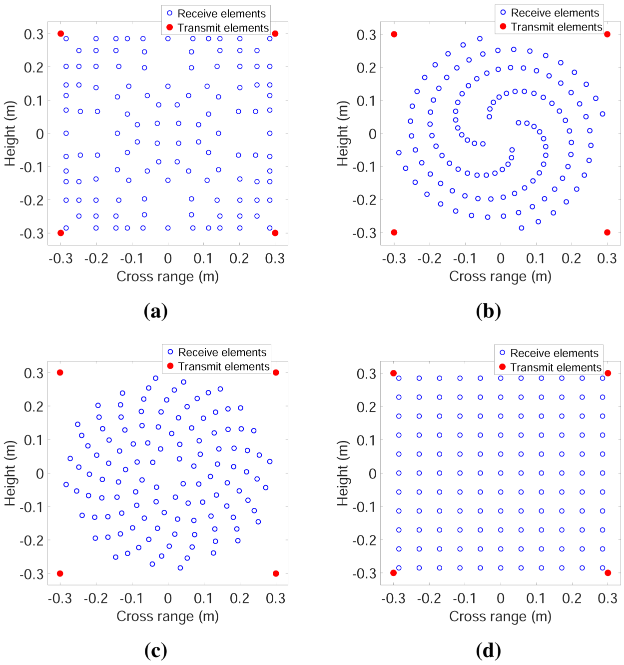

Figure 2. MIMO array topologies: (a) the synthesized sparse array, (b) the curvilinear array, (c) the spiral array, and (d) the equally spaced sparse array.

The performances of the aforementioned 2-D MIMO arrays are evaluated via the point spread functions for scatterers repectively located at the center and edge positions of the imaging scene, as shown in Figure 3. To further show the details, the cross-range projections are demonstrated in Figure 4, with the dynamic range of 60 dB. The curvilinear and spiral arrays exhibit similar focusing performances, in which we can observe strong sidelobes (about -10 dB) near the main beam in both cases. The higher sidelobes may have been caused by the circular apertures of the receive arrays. In regard to the results obtained by the optimized sparse array in this paper, in both the center and edge cases, the peak sidelobe levels are both only equal to -14.1 dB, which is much lower than those of the curvilinear and spiral arrays, but slightly larger than the sidelobe levels of the equally spaced sparse array (approximately -14.8 dB). However, in the edge case, the equally spaced sparse array exhibits much higher grating lobes (approximately -10 dB), whereas the optimized array in this work shows suppressed grating lobes smaller than -16 dB. The results indicate the efficacy of the proposed SAS method for near-field millimeter-wave imaging.

4 Conclusion

This paper proposed a convex optimization method for wideband MIMO array design for near-field imaging. An l_1-norm based optimization model was constructed, associated with a new design of the reference pattern. We compared the performance of the synthesized MIMO arrays with the state-of-the-art and commonly used sparse topologies. The numerical imaging results show that the synthesized sparse MIMO arrays in this work outperform the other arrays with regard to flexibility, sidelobe levels, and grating lobe suppression.

References

[1] S. S. Ahmed and A. Schiessl and L. Schmidt, "A Novel Fully Electronic Active Real-Time Imager Based on a Planar Multistatic Sparse Array," *IEEE Transactions on Microwave Theory and Techniques*, **59**, 12, December 2011, pp. 3567–3576, doi:10.1109/TMTT.2011.2172812.

[2] X. Zhuge and A. G. Yarovoy, "Three-Dimensional Near-Field MIMO Array Imaging Using Range Migration Techniques," *IEEE Transactions on Image Processing*, **21**, 6, June 2012, pp. 3026–3033, doi:10.1109/TIP.2012.2188036.

[3] W. F. Moulder, J. D. Krieger et al., "Development of a high-throughput microwave imaging system for concealed weapons detection," *IEEE International Symposium on Phased Array Systems and Technology*, October 2016, pp. 1–6, doi: 10.1109/ARRAY.2016.7832573.

[4] S. Li, S. Wang, M. Amin, and G. Zhao, "Efficient Near-Field Imaging Using Cylindrical MIMO Arrays," *IEEE Transactions on Aerospace and Electronic Systems*, **57**, 6, December 2021, pp. 3648–3660, doi:10.1109/TAES.2021.3079555.

[5] X. Zhuge and A. G. Yarovoy, "Study on Two-Dimensional Sparse MIMO UWB Arrays for High Resolution Near-Field Imaging," *IEEE Transactions on Antennas and Propagation*, **60**, 9, September 2012, pp. 4173–4182, doi: 10.1109/TAP.2012.2207031.

[6] Q. Cheng, Y. Liu, H. Zhang, and Y. Hao, "A Generic Spiral MIMO Array Design Method for Short-Range UWB Imaging," *IEEE Antennas and Wireless Propagation Letters*, **19**, 5, May 2020, pp. 851–855, doi: 10.1109/LAWP.2020.2982147.

[7] B. Gonzalez-Valdes et al., "Sparse array optimization using simulated annealing and compressed sensing for near-field millimeter wave imaging," *IEEE Transactions on Antennas and Propagation*, **62**, 4, April 2014, pp. 1716–1722, doi: 10.1109/TAP.2013.2290801.

[8] B. Yang, X. Zhuge, A. G. Yarovoy and L. P. Ligthart, "UWB MIMO Antenna Array Topology Design Using PSO for Through Dress Near-Field Imaging," *38th European Microwave Conference*, 2008, pp. 1620–1623, doi: 10.1109/EUMC.2008.4751782.

[9] Q. An, A. Hoorfar, H. Lv, and J. Wang, "Task-specific sparse MIMO array design for TWRI using multi-objective CMA-ES," *XXXIVth General Assembly and*

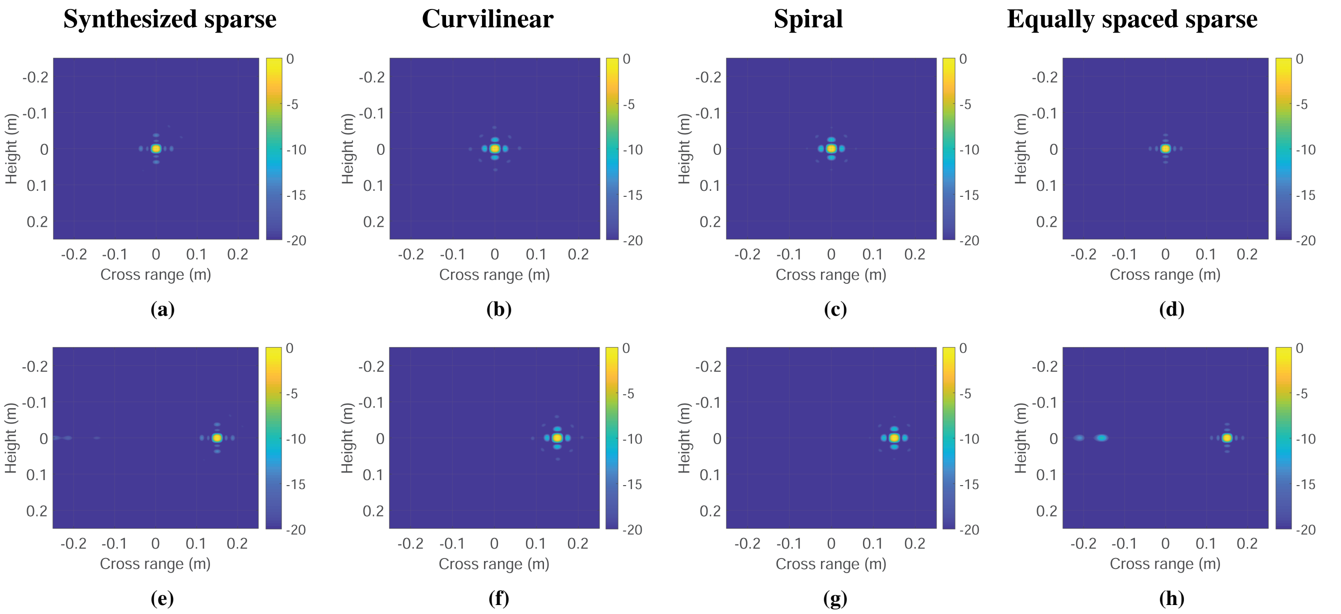

Figure 3. 2-D imaging results of the scatterer at the center position (a–d), and at the edge position (e–h). The titles on the top indicate different topologies corresponding to the images column by column.

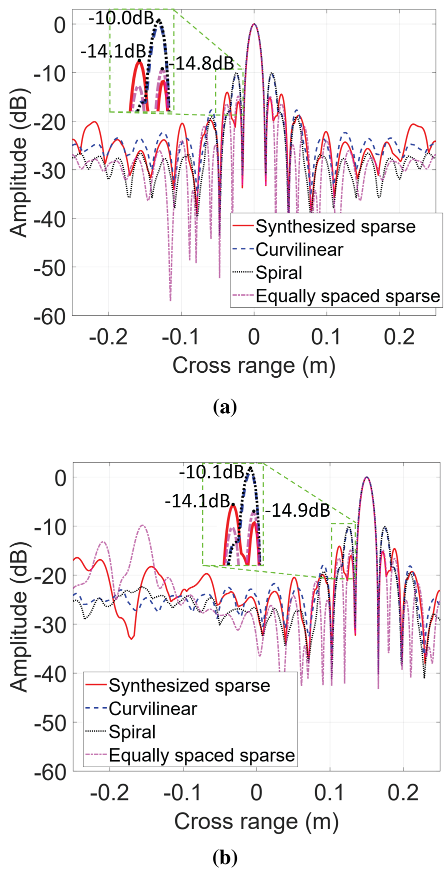

Figure 4. 1-D cross-range profiles of the scatterer at (a) the center position, and (b) the edge position.

Scientific Symposium of the International Union of Radio Science, September 2021, pp. 1–4, doi: 10.23919/URSIGASS51995.2021.9560371 .

[10] M. Hajebi and A. Hoorfar, "Multiple Buried Target Reconstruction Using a Multiscale Hybrid of Diffraction Tomography and CMA-ES Optimization," *IEEE Transactions on Geoscience and Remote Sensing*, **60**, 2022, pp. 1–13, doi:10.1109/TGRS.2022.3206722.

[11] S. M. Kay, *Fundamentals of Statistical Signal Processing: Estimation Theory*, Englewood Cliffs, N.J: Prentice-Hall PTR, 1993,

[12] D. L. Donoho and M. Elad, "Optimally sparse representation in general (nonorthogonal) dictionaries via l_1 minimization," *Proceedings of the National Academy of Sciences of the United States of America*, **100**, 5, May 2003, pp. 2197–2202, doi: 10.1073/pnas.0437847100.

[13] E. J. Candes and T. Tao, "Decoding by Linear Programming," *IEEE Transactions on Information Theory*, **51**, 12, December 2005, pp. 4203–4215, doi: 10.1109/TIT.2005.858979.

[14] E. J. Candès, M. B. Wakin, S. P. Boyd , "Enhancing Sparsity by Reweighted l_1 Minimization," *Journal of Fourier analysis and applications*, **14**, 5, December 2008, pp.877–905, doi: 10.1007/s00041-008-9045-x.

[15] M. Grant and S. Boyd, "CVX: Matlab Software for Disciplined Convex Programming, version 2.1," [Online] Available: http://cvxr.com/cvx